The Journal of Engine Research
Winter 2026, Vol. 72, No. 4, pp. 76-95
Journal Homepage: www.engineresearch.ir

Original Research

Dynamic analysis of the automotive drivetrain: comparison of Single-Mass and Dual-Mass flywheels under different operating conditions

Mohamad Taher Bayani Hedesh*, Reza Soltani, Hadi Mohammadi Bidhendi, Yaghub Abbaszadeh

Irankhodro Powertrain Company (IPCo), Tehran, Iran

ARTICLE INFO

Keywords:
Drivetrain
Conventional Clutch
Dual Mass Flywheel
Torsional Vibrations
Manual Transmission

ABSTRACT

In this study, the torsional dynamics of an automotive drivetrain equipped with a three-cylinder spark-ignition engine and a five-speed manual transmission were investigated for two configurations: a conventional single-mass flywheel (SMF) and a dual-mass flywheel (DMF). A detailed powertrain model featuring 44 torsional degrees of freedom was developed in AVL EXCITE™ PowerUnit to evaluate the influence of the DMF on vibration attenuation across a wide spectrum of operating conditions, including engine start-up, idle, vehicle launch, creep, drive and coast speed sweeps, tip-in and back-out, and engine stop. Experimental validation of the simulation results was performed for the 4th gear speed sweep of the SMF configuration. The results indicated that the DMF significantly reduced the torsional fluctuations transmitted to the gearbox in quasi-steady conditions such as idle, creep, drive and coast speed sweep. In transient conditions, however, the system exhibited more complex behavior. During start-up, stop, and launch, an increase in drivetrain oscillations and vehicle longitudinal acceleration fluctuations was observed. In contrast, in tip-in and back-out maneuvers, the DMF led to a noticeable reduction in input shaft oscillations of the gearbox. Overall, while the DMF improves powertrain torsional behavior across most quasi-steady conditions, certain transient events—particularly engine start-up—highlight limitations in its dynamic isolation capability. Furthermore, the altered inertia distribution and increased crankshaft angular velocity fluctuations necessitate additional durability and NVH assessments of cranktrain components, including the crankshaft, to ensure optimal DMF performance.

* Corresponding author
E-mail address: mt_bayani@ip-co.com (M.T. Bayani Hedesh)

Received 2 June 2026; Accepted 3 July 2026
E-ISSN: 2345-4121/ISSN: 1735-5214

Cite this article: Bayani Hedesh MT, Soltani R, Mohammadi Bidhendi H, Abbaszadeh Y. Dynamic analysis of the automotive drivetrain: comparison of Single-Mass and Dual-Mass flywheels under different operating conditions. The Journal of Engine Research. 2026 Feb 20;72(4):76-95. doi: 10.22034/ER.2026.2089785.1133

1- Introduction
Internal combustion engines, particularly three-cylinder engines, inherently produce highly fluctuating torque to internal combustion engine nature. These torque fluctuations induce torsional vibrations throughout the vehicle drivetrain [1]. Traditionally, a single-mass flywheel (SMF) used in conjunction with a clutch has served as the primary means of attenuating torsional fluctuations. However, the dual-mass flywheel (DMF) has emerged as a more advanced solution, offering a significantly improved capability to reduce vehicle vibrations and angular acceleration oscillations under a wide range of operating conditions [2].

To ensure the effective suppression of torsional irregularities by a DMF, the drivetrain must be assessed under a comprehensive set of operating conditions, including start-up, idle, launch, creep, drive and coast speed sweeps, tip-in and back-out, and stop. Each of these regimes imposes distinct dynamic demands on the system, underscoring the importance of accurate simulation for evaluating DMF performance [3–5]. In addition, key design parameters such as spring stiffness, inertia distribution, and hysteresis damping play a critical role in vibration attenuation and in maintaining smooth torque transmission with minimal oscillation [6, 7]. The evolution of DMF technology—from its early introduction in the 1980s [2] to more advanced concepts such as bifilar-type centrifugal pendulums [8] and semi-active control strategies [9]—reflects the sustained research interest and technological progress in this field.

Previous studies have extensively examined torsional vibration control in powertrains equipped with either SMFs or DMFs. Steinel [10], focusing on heavy-duty vehicles, optimized the clutch system to reduce noise and vibration, and demonstrated the contribution of the DMF to mitigating low-frequency vibrations at idle and during drive speed sweeps in different gears. Kim [11] investigated the start-up, launch, and drive behavior of vehicles equipped with continuously variable transmissions, and compared a torsion damper coupling with a DMF through both simulation and experimental testing, confirming the superior performance of the latter. Zu [9] introduced a magnetorheological fluid DMF and showed that adaptive control strategies could enhance damping performance under varying conditions such as start-up, stop, idle, drive, and coast. Chen [4] modeled the damping behavior of a DMF under start-up, idle, launch, drive, and coast conditions, with experimental results verifying the reduction in oscillatory response. Xie [5] simulated several operating conditions, including start-up, drive and coast, creep, stop, and tip-in/back-out, and validated the simulation results for the drive condition against test data. Furthermore, Wen [12] and Qu [13] extended this line of research to hybrid powertrains and heavy-duty vehicles, where drivetrain dynamics under drive conditions and in resonance zones were simulated and validated using nonlinear multi-degree-of-freedom models.

In the present study, the powertrain of a D-segment passenger vehicle equipped with a three-cylinder engine and a five-speed manual transmission is modeled with enhanced realism and improved fidelity, and the associated boundary conditions are defined accordingly. The simulation is conducted over a broad range of operating conditions, including start-up, idle, launch, drive and coast speed sweeps, tip-in and back-out, and stop, in order to compare the performance of SMF and DMF configurations under realistic operating conditions.

2- Simulation Methodology
The powertrain system—comprising a three-cylinder engine, either a conventional clutch with an SMF or a DMF, a five-speed manual transmission, and other components affecting torsional oscillations—was modeled in AVL EXCITE™ PowerUnit with 44 torsional degrees of freedom (Figure 1). Owing to the diversity of vehicle operating conditions and the torque fluctuations arising from the combined effects of combustion pressure fluctuations and

inertial forces, the drivetrain model and its corresponding boundary conditions were precisely defined.

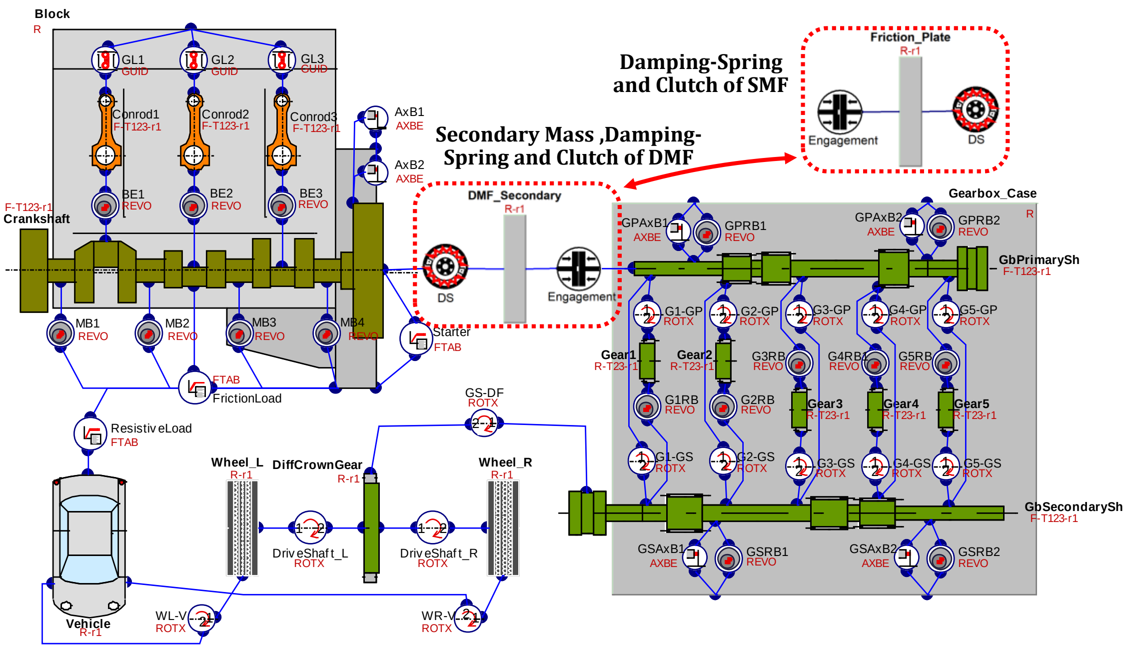

Figure 1 Powertrain system of the three-cylinder engine

2-1- Engine Load and Cranktrain

As the primary source of excitation within the drivetrain, the internal combustion engine was modeled with high fidelity by considering all components that influence the torsional vibration response of the system. The crankshaft assembly, comprising the crankshaft, the torsional vibration damper (TVD), and either the SMF or the primary mass of the DMF, was condensed using Abaqus finite element software. The condensed model was then integrated into the multibody dynamics (MBD) model in AVL EXCITE™ PowerUnit together with the engine block, connecting rods, and the remaining cranktrain components.

The combustion excitation was defined using combustion chamber pressure profiles that varied with the operating mode, ranging from full-load (Figure 2a) to motoring (no-load) conditions. In the simulation, the transient combustion pressure was applied as a concentrated force acting on the small end of the conrod. Under full-load conditions, the gas pressure fluctuations alone generated torque oscillations with an amplitude approximately 3.7 times the mean output torque of the engine (Figure 2b). Furthermore, the torsional fluctuations induced by the reciprocating inertia of the piston assembly were explicitly incorporated into the MBD model.

The spring–damper subsystem forms the principal torsional isolation mechanism within the drivetrain, mitigating angular oscillations transmitted from the engine to the transmission input shaft. In the SMF configuration, torsional compliance is provided by the clutch disc damper, where a set of coil springs arranged between the hub and friction plates supply the required stiffness and hysteresis damping. In contrast, the DMF employed in this study incorporates arc-spring assemblies located between the primary and secondary inertial masses; hence, the clutch disc contains no torsional springs and functions strictly as a friction plate. As shown in Figure 1, the geometric arrangement of the torsional isolation elements differs fundamentally between the SMF and DMF configuration. The nonlinear stiffness and hysteresis behavior of both configurations were implemented according to the characteristic curves presented in Figure 3.

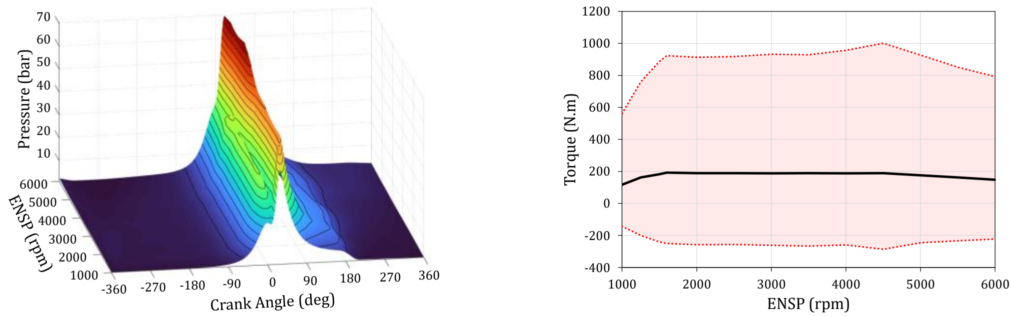

(a) (b)

Figure 2 a) Combustion chamber pressure curve and b) engine mean torque (black line) with its oscillating range (red area) under full-load conditions vs engine speed (ENSP)

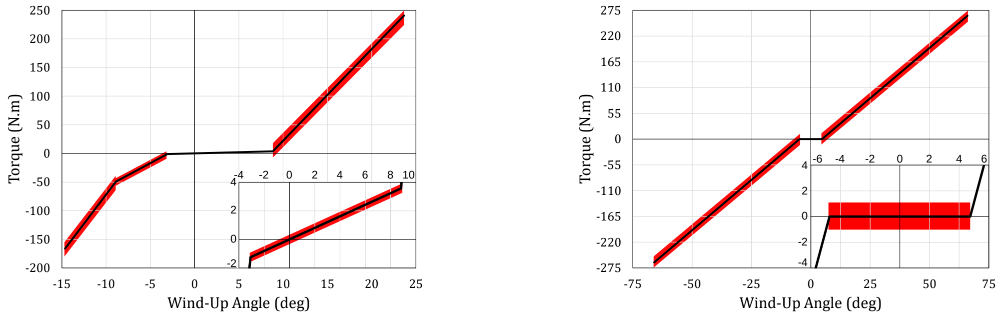

(a) (b)

Figure 3 Spring-damper characteristic curves for a) SMF and b) DMF—nominal stiffness (black line) and hysteresis friction (red region)

2-2- Transmission and Vehicle

The five-speed manual transmission was modeled by incorporating all major rotating components. The input and output shafts were condensed using Abaqus together with the components constrained to rotate with them, i.e., the fixed gears and synchronizer assemblies. The condensed shaft models were subsequently integrated into the multibody dynamics model together with all transmission gears. Depending on the selected gear, each gear was modeled in either the engaged or loose state with respect to its supporting shaft. The transmitted torque was delivered from the transmission output shaft to the differential ring gear and subsequently distributed to the left and right drive shafts with an identical speed ratio. To incorporate the damping effects of the vehicle tires, an equivalent torsional stiffness and damping were applied between the wheels and the effective moment of inertia of the vehicle body [14]. The primary drivetrain parameters are summarized in Table 1.

Table 1 Drivetrain Specifications

Index	Value	Index	Value
I_{Eng}	0.0243 kgm^2	I_{SMF}	0.1463 kgm^2
I_{DMF-P}	0.0888 kgm^2	I_{DMF-S}	0.0772 kgm^2
I_{GB-P}	0.0018 kgm^2	I_{GB-S}	43.573 kgm^2
I_W	1.0000 kgm^2	I_{Veh}	119.26 kgm^2
I_{G1}	0.0016 kgm^2	I_{G2}	0.0011 kgm^2
I_{G3}	0.0002 kgm^2	I_{G4}	0.0003 kgm^2
I_{G5}	0.0008 kgm^2	I_{Diff}	0.0155 kgm^2
K_{SMF-PD}	0.18 Nm/deg	$T_{H-SMF-PD}$	0.6 Nm
$K_{SMF-MD1}$	9.4 Nm/deg	$T_{H-SMF-MD1}$	15 Nm
$K_{SMF-MD2}$	18.8 Nm/deg	$T_{H-SMF-MD2}$	23 Nm
K_{DMF-PD}	0 Nm/deg	$T_{H-DMF-PD}$	2 Nm
K_{DMF-MD}	4.3 Nm/deg	$T_{H-DMF-MD}$	16.5 Nm
$K_{Drive-L}$	72.2 Nm/deg	$K_{Drive-R}$	67.6 Nm/deg
K_{Tyre}	446.80 Nm/deg	C_{Tyre}	12.22 Nms/deg
r_{Tyre}	299 mm	μ_{Clutch}	0.41 - 0.46
GR_1	3.45	GR_2	1.87

3- Operating Condition 1: Drive and Coast Speed Sweep

The excitation frequency of the drivetrain components—excluding the engine—varies depending on the engaged gear ratio. Furthermore, the equivalent moment of inertia of each transmission shaft changes with each gear selection, as the active gears are locked onto the shafts. Consequently, drive and coast speed sweeps must be simulated for all gear ratios [10]. To subject the drivetrain to the maximum torque fluctuation amplitude under drive operation condition, the engine speed sweep was simulated from 1,000 to 6,000 rpm under full-load conditions.

By defining appropriate resistive torques, speed sweeps were conducted in the first through fifth gears over durations of 30, 60, 90, 120, and 150 seconds, respectively, at a constant acceleration. The extended duration of the speed sweeps allowed the response oscillation amplitudes to reach their peak values at resonant frequencies, ensuring quasi-steady-state simulation conditions.

In the coast speed sweep simulation, after the system stabilized at the maximum achievable speed, the combustion chamber pressure was reduced according to the deceleration fuel cut-off (DFCO) strategy until the no-load condition was reached. Subsequently, the engine transitioned to the motoring mode, and the engine speed decreased to the minimum permissible value. The duration of the coast speed sweep was determined based on the equivalent resistive torque. The equivalent resistive torque was calculated from the engine internal mean friction, the vehicle road-load resistance on a level road (Figure 4), and the pumping losses during motoring.

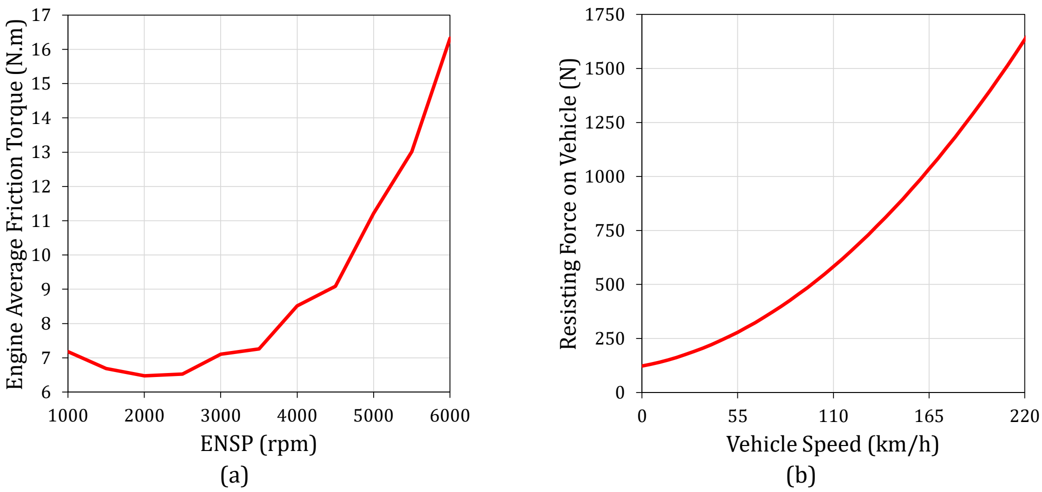

Figure 4 a) Engine friction torque during motoring at 90°C and b) resistant force acting on the vehicle on a level road

To validate the drivetrain model in the SMF configuration, the simulated fourth-gear drive speed sweep was compared against experimental test data. The angular velocity fluctuations of the crankshaft and the gearbox input shaft were measured during road testing on a track with an average gradient of 1.8°. The engine speed was increased from 1,000 to 6,000 rpm over 60 seconds under wide-open-throttle (WOT) condition, while the angular velocity fluctuations of the crankshaft and the gearbox input shaft were recorded at the same time. To ensure high resolution, the angular velocity data were acquired simultaneously at a sampling rate of 1 MHz using high-precision tachometer sensors mounted on the flywheel and at the end of the gearbox input shaft.

The simulation and experimental results for the SMF drivetrain under the drive speed sweep condition are compared in Figure 5. Good agreement was observed between the simulated and measured angular velocity fluctuations of the crankshaft and the gearbox input shaft at 1500, 3500, and 4450 rpm.

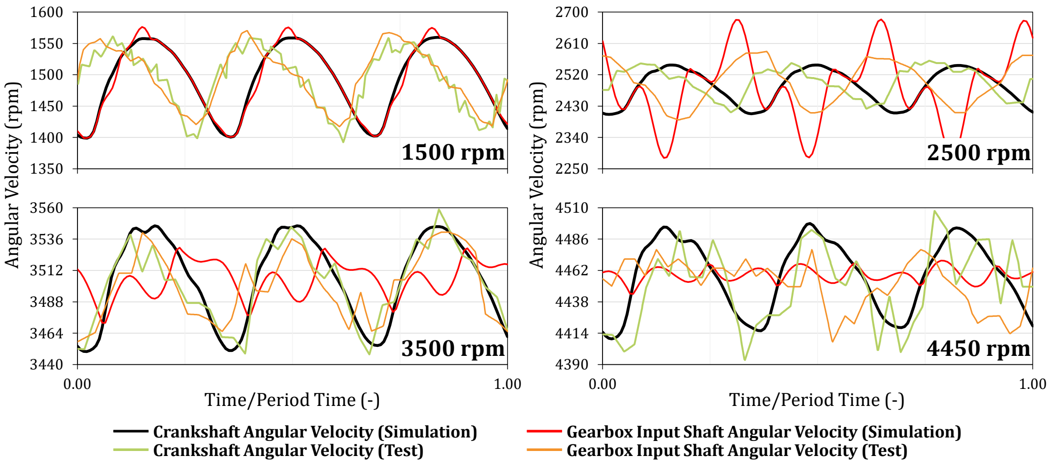

Figure 5 Dynamic response of drivetrain components equipped with SMF under simulation versus test data in 4th gear drive

At 2500 rpm, although the crankshaft oscillation trends correlate well, the standard deviation of the simulated gearbox input shaft oscillations is higher than the experimentally measured value. This discrepancy is attributed to the use of nominal values for the hysteresis friction torque in the model. Because these nominal parameters underestimate the actual hysteresis friction within the physical spring–damper assembly, the simulation overestimates the resonant response amplitude at this frequency. Figure 6 presents the dynamic response results of the simulation for the drive speed sweep from 1,000 to 6,000 rpm in fourth gear.

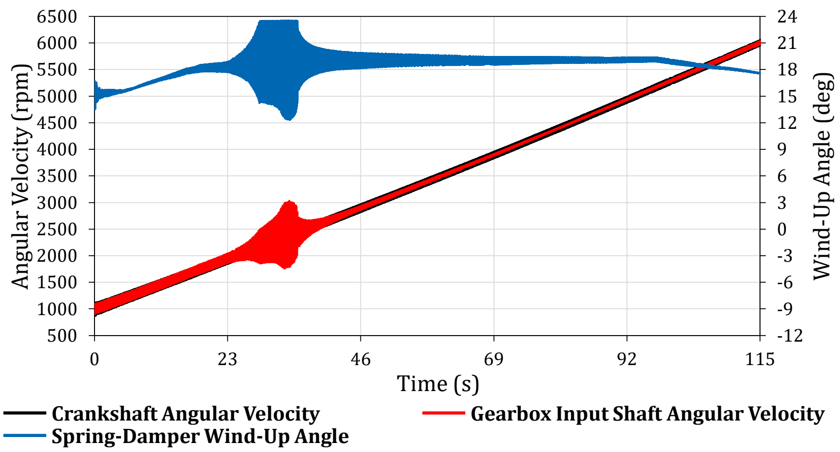

Figure 6 Dynamic response of drivetrain components equipped with SMF under 4th gear drive simulation

According to Figure 7, the angular acceleration fluctuations during the fourth-gear drive speed sweep with the SMF reached a peak amplitude of 2.3×10^5 rad/s^2 at 2360 rpm. Within this resonance region, the clutch disc spring–damper was compressed to the end of its primary damping stage. Repeated impacts against the end stop amplified the angular acceleration oscillations of the gearbox input shaft relative to those of the crankshaft. In comparison, the DMF significantly attenuates these fluctuations, limiting the angular acceleration amplitude to below 577 rad/s^2 at all speeds. Modal analysis showed that the DMF configuration reduced the first torsional natural frequency to 11.5 Hz. Consequently, the resonance shifted to approximately 460 rpm, resulting in improved torsional vibration behavior. Compared with the SMF configuration, the average angular acceleration fluctuations of the gearbox input shaft were reduced by 97%, whereas those of the crankshaft increased by 42%.

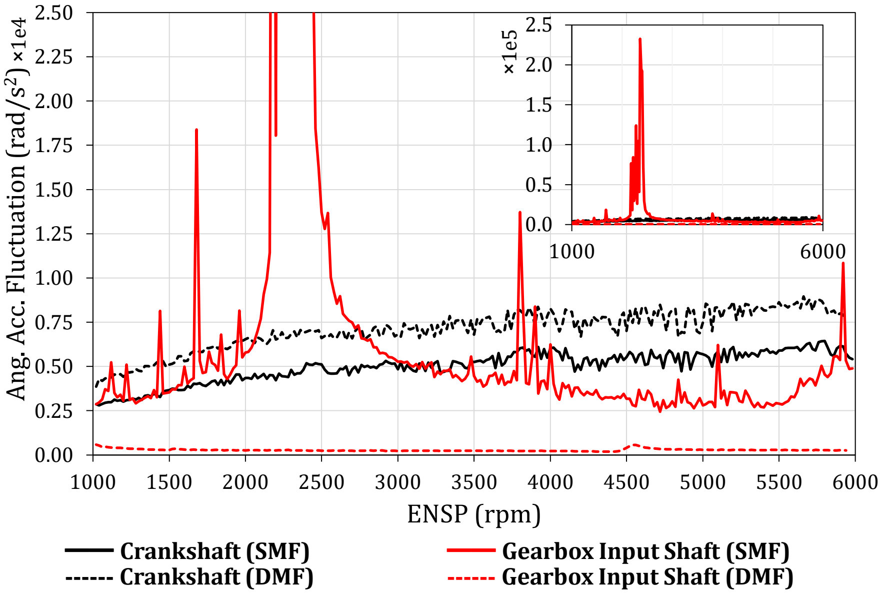

Figure 7 Angular acceleration fluctuation (orders synthesis) of drivetrain components under 4th gear drive simulation

Figure 8 compares the angular acceleration fluctuations during the second-gear drive sweep. In the SMF configuration, the angular acceleration oscillations exceed 1.5×10^5 rad/s^2 at 2560 rpm. Compared with the fourth-gear drive speed sweep, the resonance peak occurred at an engine speed approximately 8% higher in second gear. This shift resulted from a 5% reduction in the gearbox input shaft moment of inertia due to the disengagement of the fourth-gear loose gear. In the DMF configuration, the angular acceleration amplitude is limited to a maximum of 384 rad/s^2 across the full speed range. Compared with the SMF configuration, the average angular acceleration fluctuations of the gearbox input shaft were reduced by 97%, whereas those of the crankshaft increased by 43%.

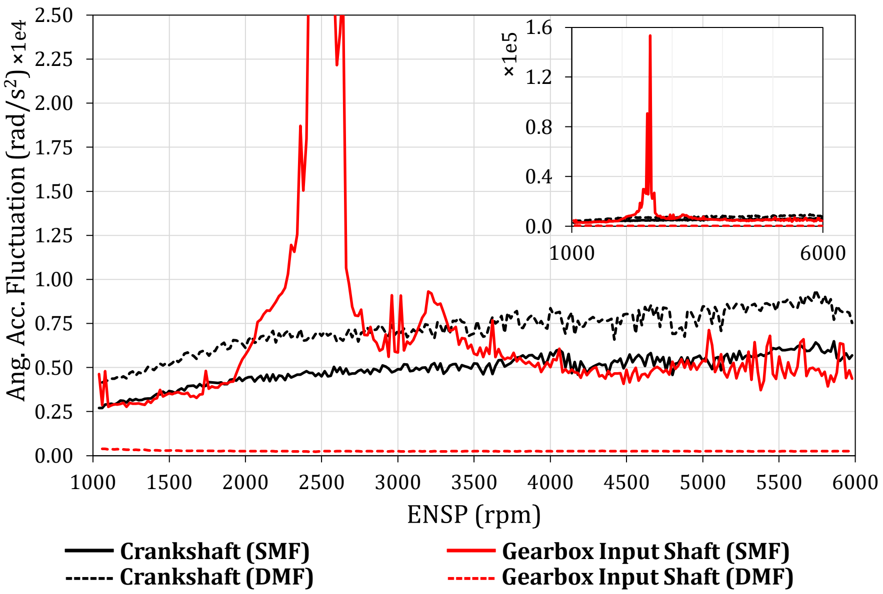

Figure 8 Angular acceleration fluctuation (orders synthesis) of drivetrain components under 2nd gear drive simulation

A closer examination of the DMF configuration during the second- and fourth-gear drive speed sweeps (Figures 7 and 8) reveals that, in fourth gear, the gearbox input shaft angular acceleration fluctuations increased by 208% at 4539 rpm relative to the adjacent engine speeds. However, this behavior was not observed in second gear. This difference is attributed to the higher transmission speed ratio in fourth gear, which excited the transmission output shaft at its resonance frequency, producing angular acceleration fluctuations of 6879 rad/s^2 that were transmitted to the gearbox input shaft. This phenomenon could not be distinguished in the SMF configuration because the high torsional oscillations of the gearbox input shaft masked its effect. Nevertheless, the resonance could still be identified in the transmission output shaft response.

During the fifth-gear coast speed sweep simulation, the engine speed for both the SMF and DMF configurations decelerated to the minimum threshold of 1576 rpm at approximately 63.5 seconds under motoring conditions. As illustrated in Figure 9, the SMF configuration exhibits significant torsional amplification, with the angular acceleration fluctuations of the gearbox input shaft reaching a peak value of 7,410 rad/s^2 and exceeding those of the crankshaft by an average of 23%. In the DMF configuration, the angular acceleration fluctuations of the gearbox input shaft remained below 487 rad/s^2 throughout the simulation. On average, they were 89% lower than those of the crankshaft.

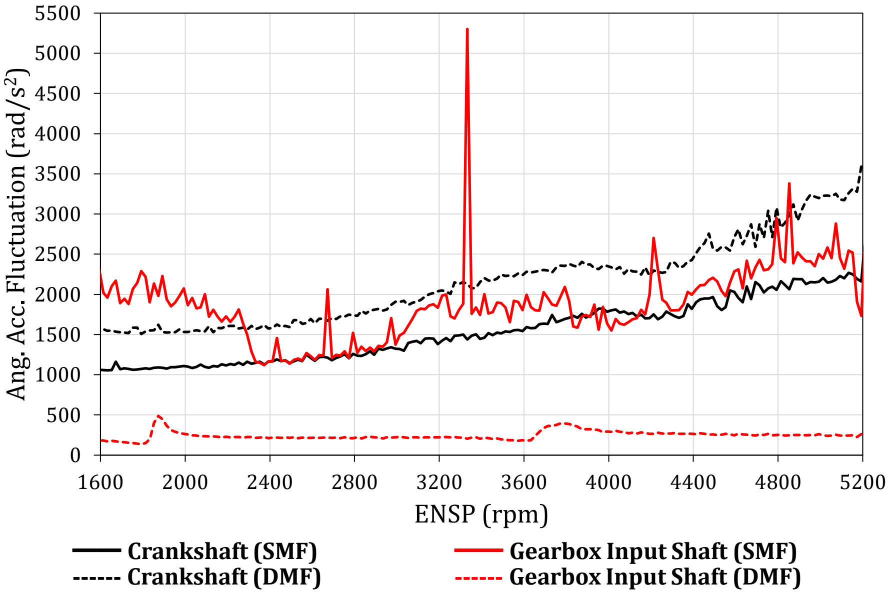

Figure 9 Angular acceleration fluctuation (orders synthesis) of drivetrain components under 5th gear coast simulation

Overall, the gearbox input shaft and crankshaft oscillations decreased by 87% and increased by 39%, respectively, in the DMF configuration compared with the SMF configuration. The reduction in torsional oscillations transmitted to the gearbox demonstrates the effectiveness of the DMF under drive and coast speed sweep operating conditions.

4- Operating Condition 2: Start-up and Idle

During the start-up simulation, the transmission was kept in neutral with the clutch fully engaged. The starter motor accelerated the crankshaft from rest. Once the engine speed reached the spark ignition threshold, the applied cylinder pressure changed from the motoring condition to the firing condition, initially producing high torque before stabilizing at a lower level.

For most DMFs, the first torsional natural frequency lies within the engine start-up speed range. Therefore, to accurately simulate this operating condition, the engine friction torque during start-up was defined as a function of crank angle under cold boundary lubrication conditions (Figure 10a), while the starter motor torque was defined as a function of engine speed (Figure 10b). As the simulation progressed, the lubrication condition transitioned to cold mixed lubrication.

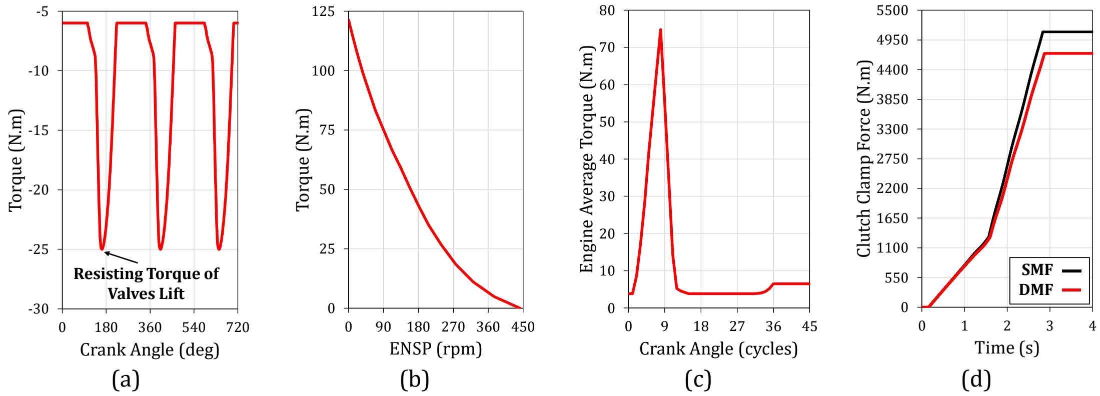

Figure 10 a) Engine friction torque under cold boundary lubrication, b) engine starter torque, c) clutch clamping force curve and d) average engine torque produced per combustion cycle during launch simulation

Figure 11 illustrates the dynamic response of the SMF drivetrain during the start-up operation condition. The engine transitioned from motoring to the firing phase at t = 0.45 s and reached an engine speed of 1,000 rpm at approximately t = 1.15 s. Prior to ignition, the engine resisting torque generated by the pumping losses induced angular velocity fluctuations during cranking. This torque had an average value of −5 N.m and ranged from −95 to 138 N.m. As a result, the initial angular velocity fluctuations exhibited a standard deviation of 54 rpm at the beginning of the start-up process.

When the transmitted torque is lower than the hysteresis friction torque of the spring–damper, the spring–damper remains in the lock-up condition and no torsional deformation occurs in the springs [15]. By simplifying the gearbox input shaft and the spring–damper into an equivalent inertia disc and a spring with Coulomb damping, the resonance region of the SMF during the pre-damping phase was determined to be between 285 and 470 rpm. Consequently, as the spring–damper exited the lock-up condition during start-up, the gearbox input shaft passed through this resonance region and experienced angular velocity resonance.

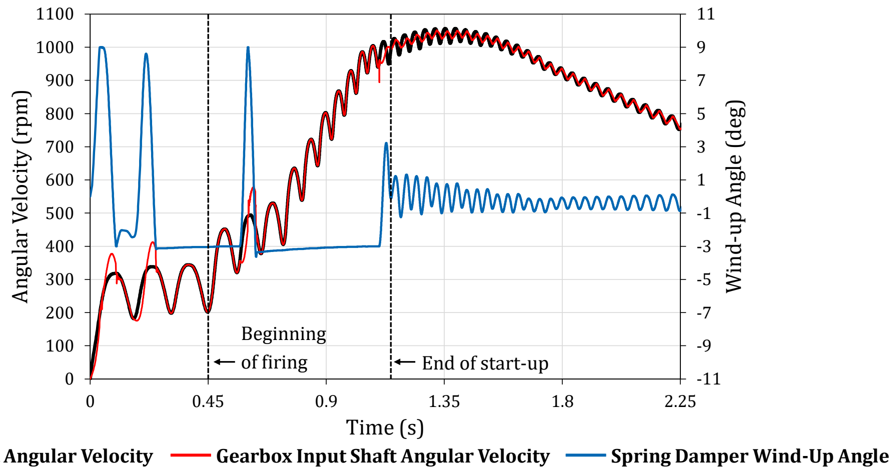

Figure 11 Dynamic response of drivetrain components equipped with SMF under simulation of start-up

Figure 12 depicts the start-up dynamic response of the DMF-equipped drivetrain. The engine speed reached 290 rpm after approximately 0.47 s of motoring. Combustion then began, and the same maximum engine torque as that used in the SMF simulation was continuously applied in an attempt to accelerate the engine to 1000 rpm. As shown, the gearbox input shaft entered a resonant state due to the torsional oscillations of the secondary mass of the DMF. These oscillations subsequently induced resonance in the crankshaft. As a result, the average crankshaft speed failed to reach 1000 rpm, preventing successful engine start-up.

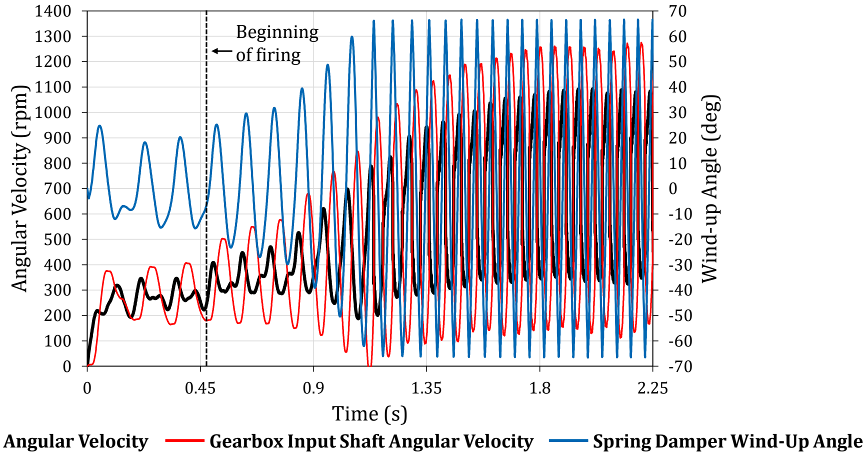

Figure 12 Dynamic response of drivetrain components equipped with DMF under start-up simulation

One common approach to overcoming the resonance region during start-up is to use a higher-power starter motor. Therefore, a starter motor with approximately three times the original power was employed. As illustrated in Figure 13, the engine speed reached 320 rpm at t = 0.37 s. Combustion then began under the same conditions as in the SMF simulation, and the engine successfully passed through the resonance region, reaching 1000 rpm at t = 1.33 s.

As shown in Figure 13, the DMF did not remain in the lock-up condition while passing through the resonance region during start-up. This behavior resulted from the lower hysteresis friction torque of the DMF relative to the moment of inertia of its secondary mass. The average cyclic standard deviations of the crankshaft and gearbox input shaft angular velocity fluctuations were 104 and 158 rpm, respectively, compared with 62 and 68 rpm for the SMF. These results indicate that the investigated DMF does not perform optimally during engine start-up.

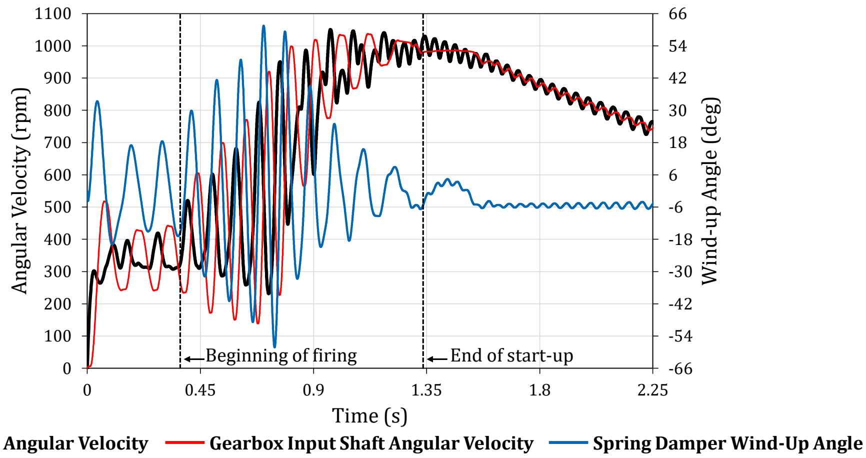

Figure 13 Dynamic response of drivetrain components equipped with DMF under start-up simulation with a starter power three times higher than the base case

To simulate the engine under idle operating conditions, the engine load was adjusted so that the combustion torque balanced the engine friction torque under mixed lubrication conditions. As a result, the average engine speed stabilized at idle (Figure 14). In the SMF and DMF configurations, the standard deviation of the crankshaft angular velocity fluctuations was 11 and 15 rpm, respectively, while the corresponding values for the gearbox input shaft were 9 and 1 rpm. Compared with the SMF, the standard deviation of the crankshaft angular acceleration fluctuations increased by 43%, whereas that of the gearbox input shaft decreased by 90% in the DMF configuration. These results indicate that the DMF provides better idle performance by significantly reducing the torsional fluctuations transmitted to the gearbox, thereby reducing the potential for gear rattle.

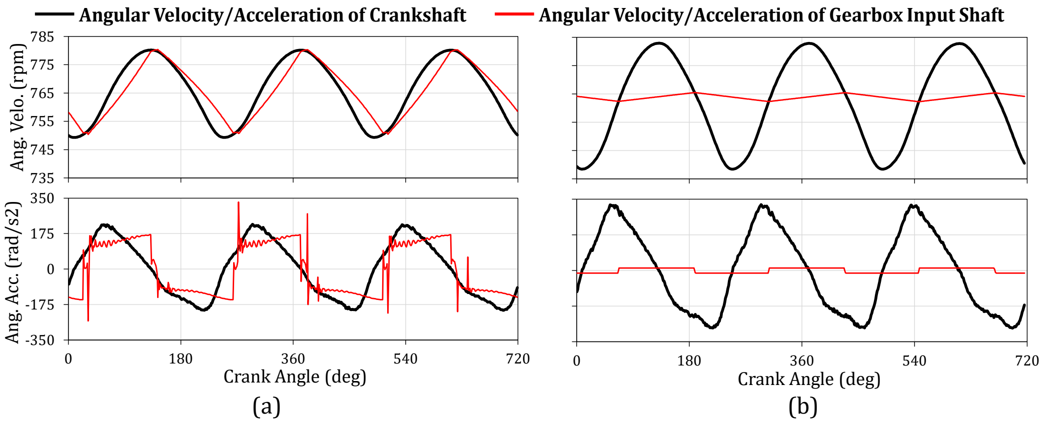

Figure 14 Dynamic response of drivetrain components equipped with a) SMF and b) DMF under idle simulation

5- Operating Condition 3: Launch and Creep

To simulate vehicle launch from standstill to creep speed, the engine was initially operated at idle speed with the transmission pre-selected in first gear and the clutch disengaged. A progressive clutch engagement was implemented over a 2.7-second interval (Figure 10c). To prevent engine stall during clutch engagement, the engine output torque was automatically increased to compensate for the vehicle resistive load (Figure 10d). Subsequently, the average angular velocities of the crankshaft and the gearbox input shaft synchronized, and the vehicle began to move, entering creep in first gear. The resistive load under this operating condition consisted of the engine friction torque under warm idle conditions and the road-load resistance acting on the vehicle on a level road (Figure 4b).

Figure 15 illustrates the dynamic response of the drivetrain with the SMF configuration during the launch operating condition. Clutch engagement began at t = 0.16 s. Before the clutch clamping force reached its maximum value, the clutch slip speed decreased to zero as the crankshaft and gearbox input shaft reached synchronous speed at t = 1.24 s. Owing to the high inertia of the drivetrain induced by clutch engagement, transient oscillations occurred, resulting in crankshaft angular velocity overshoot and undershoot of 957 and 560 rpm, respectively. These oscillations reached a steady state at t = 3.46 s.

Due to the high transmitted torque and its large fluctuations, the spring–damper rapidly transitioned from the pre-damping phase to the main damping phase. During this transition, it exited the locked state. The unlocked spring in the main damping phase caused severe instantaneous angular velocity fluctuations at the gearbox input shaft. Consequently, the average cyclic standard deviation of the angular velocity and angular acceleration fluctuations increased from 26 rpm and 257 rad/s^2 at the crankshaft to 35 rpm and 681 rad/s^2 at the gearbox input shaft, respectively.

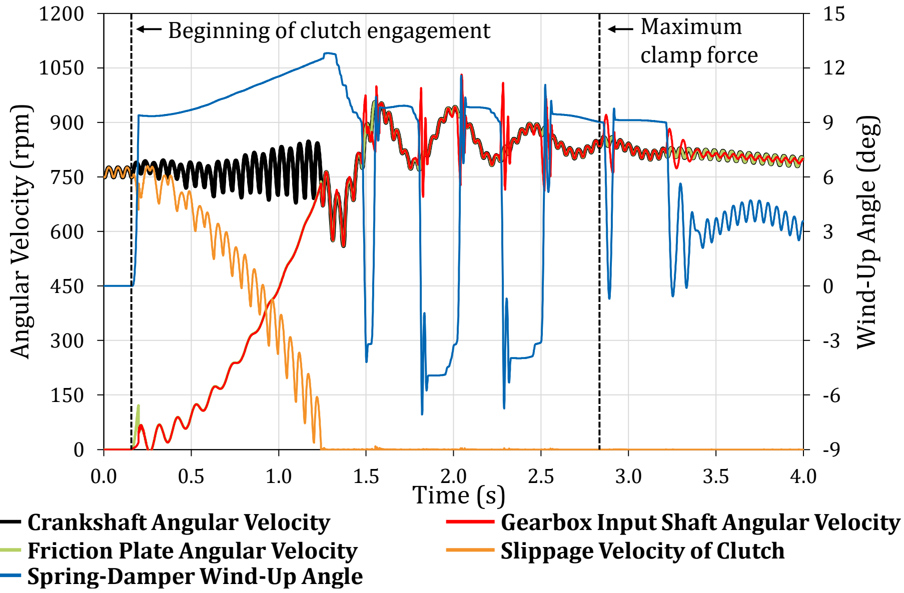

Figure 15 Dynamic response of drivetrain components equipped with SMF under launch simulation

Figure 16 presents the dynamic response of the drivetrain with the DMF configuration during the launch operating condition. The clutch engagement start time and the synchronous speed moment were identical to those in the SMF configuration. However, larger transient oscillations occurred, resulting in crankshaft angular velocity overshoot and undershoot of 1020 and 447 rpm, respectively. These oscillations reached a steady state at t = 4.06 s.

Since the launch operating condition lies above the first torsional natural frequency of the DMF, the spring–damper remained in the main damping phase throughout this operating condition. Consequently, the average cyclic standard deviation of the angular velocity and angular acceleration fluctuations changed from 36 rpm and 362 rad/s^2 at the crankshaft to 24 rpm and 98 rad/s^2 at the gearbox input shaft, respectively. Compared with the SMF configuration, the DMF effectively reduced the torsional fluctuations transmitted to the gearbox, although it increased the crankshaft oscillations.

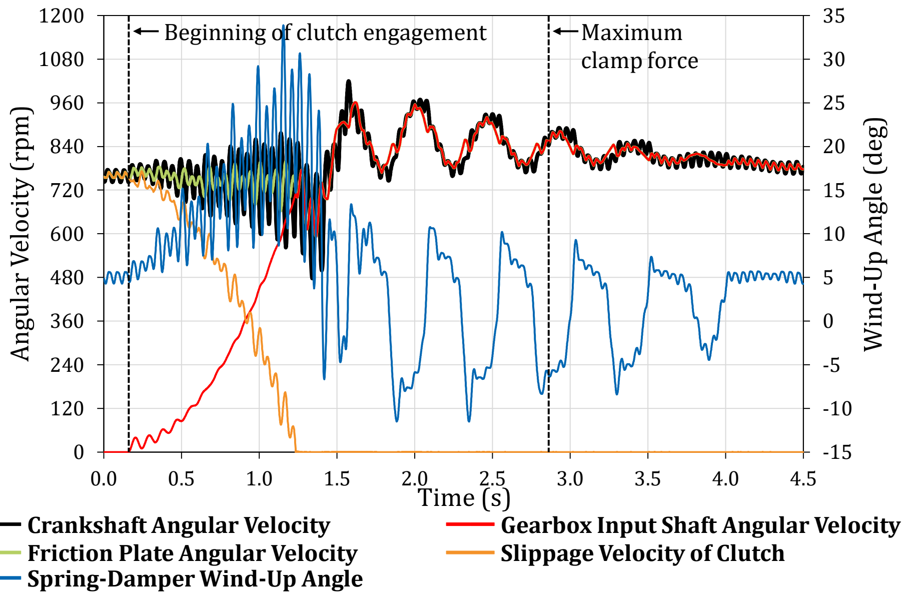

Figure 16 Dynamic response of drivetrain components equipped with DMF under launch simulation

To assess the performance of the DMF during vehicle launch, the vehicle longitudinal oscillations from t = 1.46 s until the system reached a steady state were analyzed separately. For this purpose, the torsional vibration of the equivalent disk was converted into longitudinal oscillations using the wheel radius. According to Figure 17, the standard deviations of the vehicle longitudinal acceleration and velocity increased by 31% and 30%, respectively, in the DMF configuration compared with the SMF. These results indicate that the investigated DMF adversely affected the vehicle launch performance.

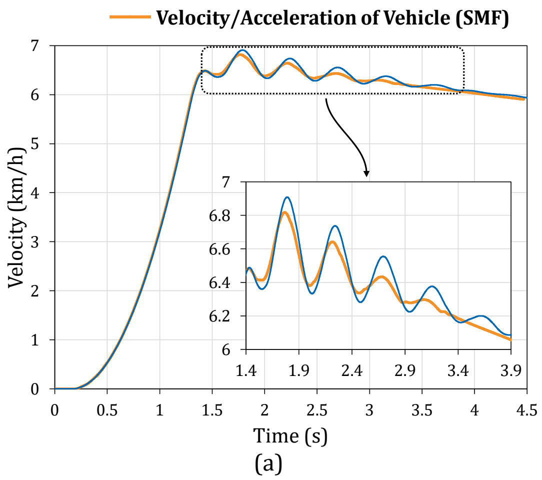

Figure 17 Longitudinal a) velocity and b) acceleration of the vehicle equipped with SMF and DMF under launch simulation

Figure 18 presents the dynamic response of the drivetrain under the first-gear creep operating condition, where the vehicle travels at a constant speed of 6 km/h. Under this operating condition, the SMF spring–damper entered the locked state, fully transmitting the engine torsional oscillations to the drivetrain. By contrast, in the DMF configuration, the spring–damper exited the locked state, reducing the angular velocity and angular acceleration fluctuations of the gearbox input shaft by 37% and 39%, respectively, relative to the crankshaft. Although the crankshaft angular velocity and angular acceleration fluctuations increased by 43% and 44%, respectively, compared with the SMF configuration, the DMF effectively attenuated the torsional oscillations transmitted to the gearbox, demonstrating superior performance under the creep operating condition.

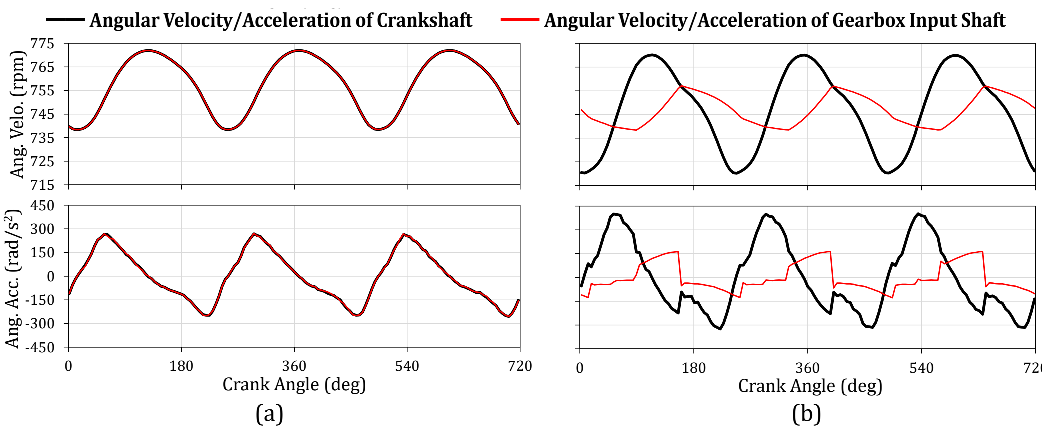

Figure 18 Dynamic response of drivetrain components equipped with a) SMF and b) DMF under 1st gear creep simulation

6- Operating Condition 4: Tip-in and Back-out

To simulate the vehicle acceleration and deceleration during the tip-in and back-out operating conditions, the vehicle was initially stabilized at a speed of 30 km/h in third-gear. During the tip-in phase, the average engine torque was gradually increased from 18 N.m at an engine speed of 1320 rpm to approximately 190 N.m, accelerating the vehicle to 60 km/h. Subsequently, the back-out phase was initiated. As the engine speed reached 2650 rpm, the average engine torque was gradually reduced from 189 N.m to an engine-braking torque of −10 N.m, causing the vehicle to decelerate to 30 km/h, where it was stabilized by appropriate torque adjustment (Figure 19). The resistive loads considered in this operating condition consisted of the average engine friction torque (Figure 4a), the road-load resistance on a level road (Figure 4b), and the pumping-loss torque during motoring.

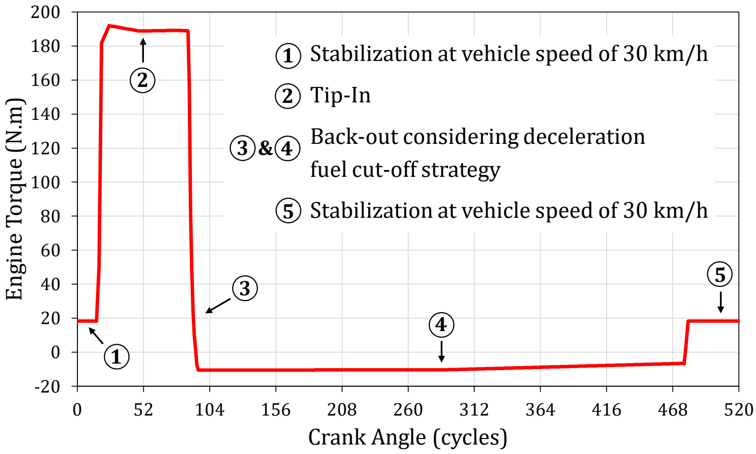

Figure 19 Average engine torque produced per cycle during 3rd-gear tip-in and back-out simulation

Figure 20 illustrates the dynamic response of the drivetrain with the SMF configuration during the third-gear tip-in and back-out operating conditions. During the tip-in phase, transient oscillations in the crankshaft angular velocity resulted in overshoot and undershoot of 1501 and 1207 rpm, respectively. Before the system reached a steady state at t = 1.32 s, the average cyclic standard deviation of the angular velocity and angular acceleration fluctuations was 66 rpm and 1695 rad/s^2 at the crankshaft, and 72 rpm and 3306 rad/s^2 at the gearbox input shaft, respectively.

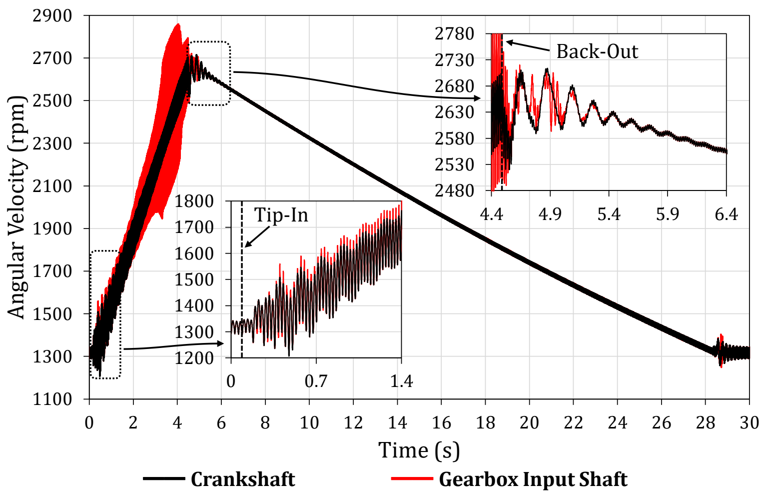

Figure 20 Dynamic response of drivetrain components equipped with SMF under 3rd-gear tip-in and back-out simulation

During the back-out phase in the SMF configuration, transient oscillations again occurred, resulting in crankshaft angular velocity overshoot and undershoot of 2714 and 2520 rpm, respectively. Before the system reached a steady state at t = 5.49 s, the average cyclic standard deviation of the angular velocity and angular acceleration fluctuations was 13 rpm and 295 rad/s^2 at the crankshaft, and 17 rpm and 701 rad/s^2 at the gearbox input shaft, respectively.

Figure 21 presents the dynamic response of the drivetrain with the DMF configuration during the third-gear tip-in and back-out operating conditions. During the tip-in phase, transient oscillations in the crankshaft angular velocity resulted in overshoot and undershoot of 1565 and 1145 rpm, respectively. Before the system reached a steady state at t = 1.74 s, the average cyclic standard deviation of the angular velocity and angular acceleration fluctuations was 99 rpm and 2639 rad/s^2 at the crankshaft, and 17 rpm and 195 rad/s^2 at the gearbox input shaft, respectively. Compared with the SMF configuration, the crankshaft experienced more severe transient oscillations, while the gearbox input shaft oscillations were significantly reduced.

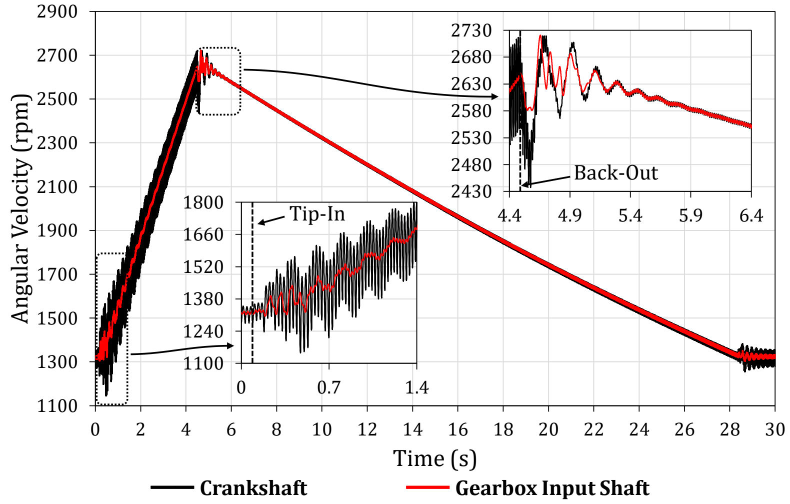

Figure 21 Dynamic response of drivetrain components equipped with DMF under 3rd-gear tip-in and back-out simulation

During the back-out phase in the DMF configuration, transient oscillations again occurred, resulting in crankshaft angular velocity overshoot and undershoot of 2719 and 2437 rpm, respectively. Before the system reached a steady state at t = 5.41 s, the average cyclic standard deviation of the angular velocity and angular acceleration fluctuations was 16 rpm and 424 rad/s^2 at the crankshaft, and 11 rpm and 104 rad/s^2 at the gearbox input shaft, respectively. Compared with the SMF configuration, larger transient oscillations occurred at the crankshaft, whereas the gearbox input shaft experienced substantially lower fluctuations.

Figure 22 presents the vehicle longitudinal acceleration response during the third-gear tip-in and back-out operating conditions. The results show that, compared with the SMF configuration, the average cyclic standard deviation of the vehicle longitudinal acceleration fluctuations decreased by 43% during the tip-in phase, whereas it increased by 3% during the back-out phase in the DMF configuration.

Considering the results of the tip-in and back-out operating conditions, the DMF demonstrated excellent performance in reducing the torsional vibrations transmitted to the gearbox. Although it caused a slight increase in the vehicle longitudinal acceleration fluctuations during the back-out phase, this increase was negligible compared with the substantial reduction in the torsional vibrations transmitted through the drivetrain.

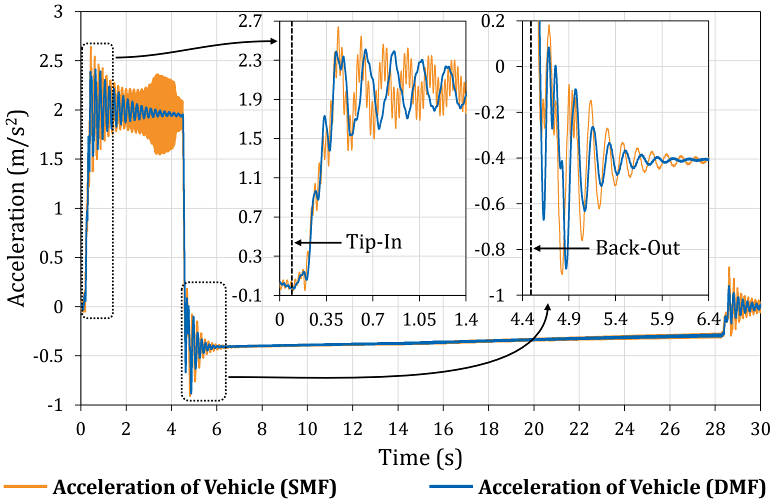

Figure 22 Longitudinal acceleration of vehicle equipped with SMF and DMF under 3rd-gear tip-in and back-out simulation

7- Operating Condition 5: Stop

To simulate the engine stop operating condition, the engine was initially stabilized at idle speed with the transmission in neutral and the clutch engaged. The engine then transitioned from firing to the motoring condition. Under the action of the resistive loads, the engine speed gradually decreased, passed through the first torsional resonance region of the system spring-damper, and eventually came to a stop. The resistive loads considered in this simulation consisted of the engine friction torque under warm mixed-lubrication conditions, using the same modeling approach as in the start-up operating condition, together with the engine pumping-loss torque during motoring.

Figure 23 presents the dynamic response of the drivetrain with the SMF configuration during the engine stop operating condition. The engine came to a complete stop 2.07 s after combustion ceased. Similar to the start-up operating condition, as the crankshaft speed passed through the resonance region of the spring–damper pre-damping phase, the gearbox input shaft oscillations were amplified as the spring–damper exited the locked state. From the end of combustion until the engine first came to a stop at t = 1.31 s, the average cyclic standard deviation of the angular velocity fluctuations was 40 rpm at the crankshaft and 38 rpm at the gearbox input shaft.

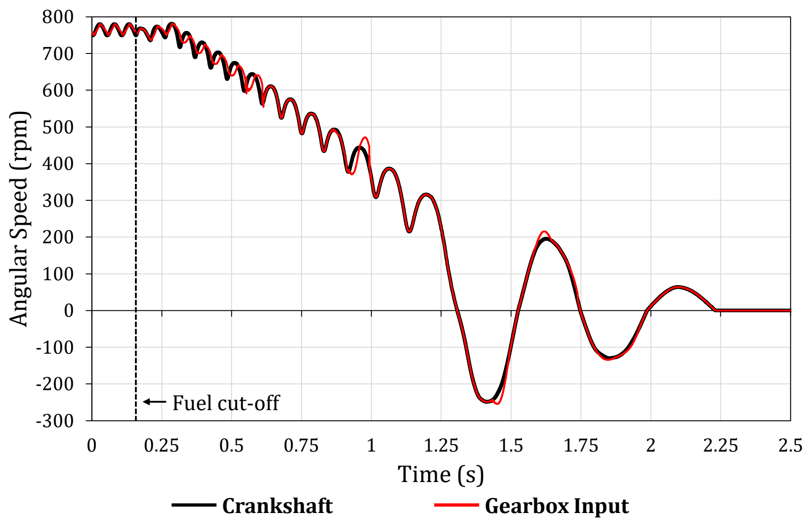

Figure 23 Dynamic response of drivetrain components equipped with SMF under Stop simulation

Figure 24 shows the dynamic response of the drivetrain with the DMF configuration during the engine stop operating condition. The engine reached a complete stop 2.21 s after combustion ceased. As the engine speed passed through the natural frequency of the main damping phase, the gearbox input shaft angular velocity oscillations increased to values 33% higher than those of the crankshaft. From the end of combustion until the engine first stopped at t = 1.37 s, the average cyclic standard deviation of the angular velocity fluctuations was 49 rpm at the crankshaft and 55 rpm at the gearbox input shaft.

These findings indicate that the investigated DMF did not provide satisfactory performance during the stop operating condition. The resulting increase in torsional oscillations has the potential to aggravate engine and drivetrain NVH, with gearbox rattle being one of the most likely consequences.

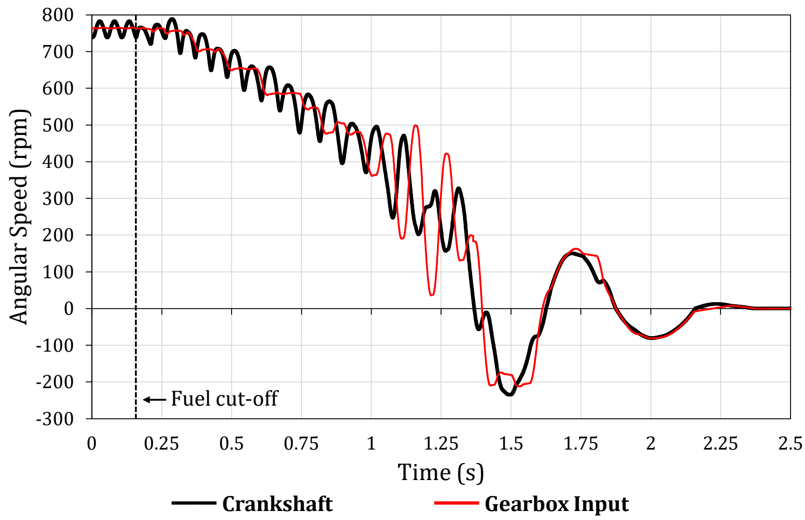

Figure 24 Dynamic response of drivetrain components equipped with DMF under Stop simulation

8- Conclusion

In this study, the drivetrain of a three-cylinder engine was modeled in both single-mass flywheel (SMF) and dual-mass flywheel (DMF) configurations and evaluated under drive and coast speed sweep, start-up, idle, launch, creep, tip-in and back-out, and stop operating conditions.

The results showed that the DMF provided excellent torsional vibration isolation under quasi-steady operating conditions, including drive and coast speed sweep, idle, and creep. In these operating conditions, the torsional oscillations transmitted to the gearbox input shaft were reduced by more than 90% compared with the SMF configuration. During tip-in, the DMF also effectively reduced the torsional oscillations transmitted to the gearbox, while only a slight increase in vehicle longitudinal oscillations was observed during back-out.

However, under highly transient operating conditions, the performance of the investigated DMF was strongly influenced by resonance crossing. During start-up, the engine speed passed through the first torsional natural frequency of the DMF main damping stage, resulting in severe torsional oscillations that prevented successful engine start-up with the standard starter motor. Therefore, a higher-power starter motor was required to overcome the resonance region. A similar phenomenon was observed during the engine stop operating condition, where passing through the same resonance region increased the crankshaft and gearbox input shaft oscillations, resulting in unsatisfactory DMF performance. During launch, although the DMF significantly reduced the torsional oscillations transmitted to the gearbox, it increased the longitudinal oscillations of the vehicle.

The identified limitations of the investigated DMF in reducing torsional vibrations transmitted to the gearbox under transient operating conditions indicate that further optimization of the DMF design is required. In addition, the increase in crankshaft torsional oscillations and the redistribution of mass and inertia between the crankshaft flange and the gearbox input shaft resulting from replacing the conventional flywheel and clutch assembly with a DMF assembly may alter the mechanical loading of drivetrain components. Therefore, a comprehensive structural durability assessment should be conducted to evaluate the resulting stress distribution and ensure the long-term reliability of critical drivetrain components.

List of Symbols

I_{Eng}	Effective engine inertia without flywheel
I_{SMF}	Inertia of Single Mass Flywheel (SMF) and clutch assembly
I_{DMF-P}	Inertia of the primary part of the Dual Mass Flywheel (DMF)
I_{DMF-S}	Inertia of the secondary part of the DMF and clutch assembly
I_{GB-P}	Inertia of the gearbox input shaft
I_{GB-S}	Inertia of the gearbox output shaft
I_W	Inertia of the wheel
I_{Veh}	Effective inertia of the vehicle
I_{GX}	Inertia of the x-th gear
I_{Diff}	Inertia of the differential gear
K_{XMF-PD}	Torsional stiffness of the spring damper - pre-damping stage
K_{XMF-MD}	Torsional stiffness of the spring damper - main damping stage
$T_{H-XMF-XD}$	Hysteresis frictional torque of each spring damper stage
$K_{Drive-X}$	Torsional stiffness of the right/left drive shaft
K_{Tyre}	Torsional stiffness of the tire
C_{Tyre}	Torsional damping of the tire
μ_{Clutch}	Friction coefficient of the clutch plate
r_{clutch}	Effective radius of the clutch
X_{GRX}	Speed ratio of driven to driving gear in x-th gear

References

[1] Wang P, Li G, Li X. Vibration characteristics analysis of o-shaped damping ring to balance damping gear transmission system for three-cylinder engine. Processes. 2022 Aug 25;10(9):1685. doi: 10.3390/pr10091685

[2] Sebulke A. The two-mass flywheel-a torsional vibration damper for the power train of passenger cars-state of the art and further technical development. InSAE International Congress and Exposition 1987 Feb 1. SAE Technical Paper. doi: 10.4271/870394

[3] Fidlin A, Seebacher R. DMF simulation techniques. In8th LuK symposium 2006 (p. 55).

[4] Chen L, Shi W, Chen Z. Research on damping performance of dual mass flywheel based on vehicle transmission system modeling and multi-condition simulation. IEEE Access. 2020 Feb 13;8:28064-77. doi: 10.1109/ACCESS.2019.2951618

[5] Xie M, Wang S, Yan Z, Wang L, Tan G. Optimization of Dual-Mass Flywheel Parameters Based on a Multicondition Simulation Test. Shock and Vibration. 2022;2022(1):2954825. doi: 10.1155/2022/2954825

[6] Albers A. Advanced development of dual mass flywheel (DMFW) design-noise control for today's automobiles. InProceedings of the 5th LuK Symposium 1994 May (pp. 5-41).

[7] Luo H, Wu G, Wu Q, Zhan W, Yang J, Xu L. Research on the Design Method and Vibration Reduction Performance of Dual-Mass Flywheel. InSociety of Automotive Engineers (SAE)-China Congress 2018 Nov 6 (pp. 499-512). Singapore: Springer Singapore. doi: 10.1007/978-981-13-9718-9_37

[8] Chen L, Yuan J, Cai H, Hu J. Dynamic Model and Dynamic Response of Automobile Dual-Mass Flywheel with Bifilar-Type Centrifugal Pendulum Vibration Absorber. Shock and Vibration. 2021;2021(1):6627938. doi: 10.1155/2021/6627938

[9] Zu QH, Chen ZY, Shi WK, Mao Y, Chen ZY. Torsional vibration semiactive control of drivetrain based on magnetorheological fluid dual mass flywheel. Mathematical Problems in Engineering. 2015;2015(1):608737. doi: 10.1155/2015/608737

[10] Steinel K. Clutch tuning to optimize noise and vibration behavior in trucks and buses. InInternational Mobility Technology Conference and Exhibit 2000 Dec 1. SAE Technical Paper. doi: 10.4271/2000-01-3292

[11] Kim J. Launching performance analysis of a continuously variable transmission vehicle with different torsional couplings. J. Mech. Des.. 2005 Mar 1;127(2):295-301. doi: 10.1115/1.1814387

[12] Wen Z, Guo B, Nie H, Chen L, Liu S, Yan Z. Torsional Vibration Characteristics Analysis and Parameter Optimization of Parallel Hybrid Electric Vehicle Powertrain. Shock and Vibration. 2024;2024(1):1711480. doi: 10.1155/vib/1711480

[13] Qu J, Shi W, Chen Z, Yuan R, Liu J, Zhao Y, Guo N. Nonlinear modeling and torsional vibration analysis of heavy-duty vehicle powertrain system during acceleration. Advances in Mechanical Engineering. 2024 Jul;16(7):16878132241263936. doi: 10.1177/16878132241263936

[14] Crowther A, Zhang N, Liu DK, Jeyakumaran JK. Analysis and simulation of clutch engagement judder and stick-slip in automotive powertrain systems. Proceedings of the Institution of Mechanical Engineers, Part D: Journal of Automobile Engineering. 2004 Dec 1;218(12):1427-46. doi: 10.1243/0954407042707731

[15] Szadkowski A, Prange E, Naganathan NG. Hysteresis effects on driveline torsional vibrations. SAE Technical Paper; 1995 May 1. doi: 10.4271/951293

نشریه علمی تحقیقات موتور
زمستان ۱۴۰۴، جلد ۷۲، شماره ۴، صفحه ۷۶-۹۵
تارنمای نشریه: www.engineresearch.ir
مقاله پژوهشی

تحلیل دینامیکی زنجیره انتقال قدرت خودرو: مقایسه چرخ‌لنگر تک‌جرمی و دوجرمی در شرایط عملیاتی مختلف

محمد طاهر بیانی هدش*، رضا سلطانی، هادی محمدی بیدهندی، یعقوب عباس‌زاده

شرکت تحقیق، طراحی و تولید موتور ایران خودرو (ایپکو)، تهران، ایران

اطلاعات مقاله

کلیدواژه‌ها:
زنجیره انتقال قدرت
کلاچ متداول
چرخ‌لنگر دوجرمی
نوسانات پیچشی
جعبه‌دنده دستی

چکیده

در این پژوهش، رفتار دینامیکی زنجیره انتقال قدرت یک خودروی سواری مجهز به موتور سه‌استوانه و جعبه‌دنده پنج‌سرعته دستی، در دو پیکربندی چرخ‌لنگر تک‌جرمی و دوجرمی شبیه‌سازی و مقایسه شده است. هدف، ارزیابی میزان تأثیر چرخ‌لنگر دوجرمی بر کاهش نوسانات پیچشی و ارتعاشات انتقال‌یافته به جعبه‌دنده و مجموعه خودرو تحت شرایط گوناگون عملیاتی است. برای این منظور، الگوی جامع سامانه انتقال قدرت با ۴۴ درجه آزادی پیچشی در نرم‌افزار AVL EXCITE™ PowerUnit توسعه یافت و مجموعه گسترده‌ای از حالات عملیاتی شامل راه‌اندازی، دور آرام، آغاز حرکت، خزش، جاروب‌های افزایش و کاهش سرعت، شتاب‌گیری آنی مثبت و منفی و توقف تحلیل شد. علاوه بر این، نتایج شبیه‌سازی در دنده چهار برای شرایط جاروب سرعت با داده‌های آزمون تجربی اعتبارسنجی شد. نتایج نشان می‌دهد که چرخ‌لنگر دوجرمی در شرایط شبه‌پایدار نظیر دور آرام، خزش و جاروب‌های سرعت، به‌طور قابل‌توجهی دامنه نوسانات ورودی به جعبه‌دنده را کاهش می‌دهد. در مقابل، در حالات گذرای شدید، رفتار سامانه پیچیده‌تر بوده و در شرایط عملیاتی راه‌اندازی، توقف و آغاز حرکت، افزایش نوسانات ورودی به جعبه‌دنده و شتاب خطی خودرو مشاهده می‌شود. با این حال، در آزمون‌های شتاب‌گیری آنی مثبت و منفی، چرخ‌لنگر دوجرمی کاهش محسوس نوسانات محور ورودی جعبه‌دنده را به همراه دارد. به‌طور کلی، استفاده از چرخ‌لنگر دوجرمی موجب بهبود رفتار دینامیکی زنجیره انتقال قدرت می‌شود؛ هرچند در برخی شرایط گذرای خاص مانند راه‌اندازی، کارایی آن با محدودیت همراه است. همچنین افزایش نوسانات سرعت زاویه‌ای میل‌لنگ و تغییر توزیع گشتاور لختی میان میل‌لنگ و محور ورودی جعبه‌دنده، ضرورت انجام تحلیل‌های تکمیلی برای اجزایی نظیر میل‌لنگ را برجسته می‌سازد.

* نویسنده مسئول
پست الکترونیکی: mt_bayani@ip-co.com (محمد طاهر بیانی هدش)

دریافت ۱۲ خرداد ۱۴۰۵؛ پذیرش ۱۲ تیر ۱۴۰۵
شاپای الکترونیکی: ۴۱۲۱-۲۳۴۵ / شاپای چاپی: ۵۲۱۴-۱۷۳۵

Cite this article: Bayani Hedesh MT, Soltani R, Mohammadi Bidhendi H, Abbaszadeh Y. Dynamic analysis of the automotive drivetrain: comparison of Single-Mass and Dual-Mass flywheels under different operating conditions. The Journal of Engine Research. 2026 Feb 20;72(4):76-95. doi: 10.22034/ER.2026.2089785.1133